Regional anthropogenic aerosol reductions amplify probability of record-breaking heat extremes

Florian Kraulich[1,*], Peter Pfleiderer[1], Sharar Ahmadi[2], Robert J. Allen[3], Pierre Nabat[4], Geeta G. Persad[5], Bjørn H. Samset[6], Laura J. Wilcox[2] and Sebastian Sippel[1]

[1]Institute for Meteorology, Leipzig University; Leipzig, Germany

[2]National Centre for Atmospheric Science, University of Reading; Reading, United Kingdom

[3]Department of Earth and Planetary Sciences, University of California Riverside; Riverside CA, USA

[4]Météo-France, CNRS, Univ. Toulouse, CNRM; Toulouse, France

[5]Department of Earth and Planetary Science, The University of Texas at Austin; Austin, USA

[6]CICERO Center for International Climate Research; Oslo, Norway

[*]Corresponding author: florian.kraulich@uni-leipzig.de

This is a non-peer-reviewed preprint submitted to EarthArXiv. The manuscript was submitted to *Environmental Research: Climate*.

Environmental Research: Climate

Crossmark

PAPER

Regional anthropogenic aerosol reductions amplify probability of record-breaking heat extremes

Florian Kraulich[1,*], Peter Pfleiderer[1], Sharar Ahmadi[2], Robert J. Allen[3], Pierre Nabat[4], Geeta G. Persad[5], Bjørn H. Samset[6], Laura J. Wilcox[2] and Sebastian Sippel[1]

[1]Institute for Meteorology, Leipzig University; Leipzig, Germany
[2]National Centre for Atmospheric Science, University of Reading; Reading, United Kingdom
[3]Department of Earth and Planetary Sciences, University of California Riverside; Riverside CA, USA
[4]Météo-France, CNRS, Univ. Toulouse, CNRM; Toulouse, France
[5]Department of Earth and Planetary Science, The University of Texas at Austin; Austin, USA
[6]CICERO Center for International Climate Research; Oslo, Norway
*Author to whom any correspondence should be addressed.

E-mail: florian.kraulich@uni-leipzig.de

RECEIVED
dd Month yyyy

REVISED
dd Month yyyy

Keywords: Heat extremes, aerosols, record statistics, record-breaking extremes, RAMIP

Abstract

Record-breaking heat extremes are becoming more likely due to anthropogenic climate change, with their probability depending on the regional warming rate. Anthropogenic aerosol forcing modulates these warming rates, and aerosols are declining globally. However, the influence of aerosols on the probability of record-breaking heat extremes remains unclear. Here, we assess how aerosol trends alter record-breaking heat probabilities by combining idealized simulations, CESM2 large ensemble and single-forcing large ensemble simulations, Regional Aerosol Model Intercomparison Project (RAMIP) future aerosol scenarios, and ERA5/MERRA-2 reanalysis data. Reanalysis data provide empirical evidence for a link between changes in aerosol concentrations and record-breaking heat extremes. There is a statistically significant correlation between changes in sulfate aerosol optical depth (SO_4AOD) and record occurrence after accounting for latitudinal differences in record probability, with a 0.5 percentage points increase in annual record-breaking probability for every 10% decrease in SO_4AOD. For context, the global land-mean annual record-breaking probability during 2010–2025 is 6.7%. Consistent with this empirical relationship, idealized simulations show that increased warming rates can lead to higher record-breaking probabilities, with a lagged response. In CESM2, present-day record-breaking probabilities are amplified relative to GHG-only across most of the world, e.g. by 67% in Central Europe where aerosol forcing declines, whereas they are damped by 47% in South Asia where aerosol forcing increases. RAMIP simulations show that aerosol reductions would increase record-breaking probabilities, especially in regions with high remaining aerosol concentrations. For example, reducing global anthropogenic aerosol emissions from SSP3-7.0 to SSP1-2.6 results in an annual record-breaking heat probability of 11.4% instead of 6.7% in parts of South Asia in the 2040s. These results show that regional aerosol trends can substantially modulate record-breaking heat extremes by altering regional warming rates. Aerosol reductions can therefore temporarily amplify record-breaking heat probabilities, although greenhouse gas forcing remains the dominant driver of long-term increases.

1 Introduction

Heat extremes are becoming more frequent and more intense due to anthropogenic climate change (Perkins-Kirkpatrick & Lewis 2020, Seneviratne et al. 2021, Engdaw et al. 2023), increasing the probability of new heat records (Rahmstorf & Coumou 2011, Fischer et al. 2025). Record-breaking heat extremes can have strong impacts on societies because communities are adapted to their local climate (Tobías et al. 2021). Thus, communities are often not prepared for events outside their previous experience, resulting in higher vulnerability and therefore higher impacts (Thompson

et al. 2023). Heat-related excess deaths increase non-linearly with rising temperatures above the optimal temperature (Gasparrini et al. 2015). Looking at record-breaking heat extremes locally helps to take local adaptation into account because records are defined relative to past climate conditions at the local level. Still, the impacts of locally defined records can differ strongly between regions, depending on absolute temperature and humidity (Mora et al. 2017).

The annual probability of record-breaking heat extremes depends on the warming rate (Wergen & Krug 2010, Fischer et al. 2025). The higher the warming rate, the higher the probability of a record-breaking extreme. In a stationary climate without warming, the probability of new records declines as the time series gets longer and approaches zero for long time series. For a positive warming rate, the annual record-breaking probability converges to a constant that depends on the warming rate and internal variability (Wergen & Krug 2010, Rahmstorf & Coumou 2011). Due to greenhouse gas (GHG)-induced global warming, the warming rate has been positive in recent decades (Gulev, S. K. et al. 2021, Forster et al. 2025). However, regional warming rates are not only determined by GHG-induced global warming but can also be modulated by regional forcings such as aerosols.

Aerosols are small liquid or solid particles in the atmosphere that can originate naturally, e.g. from sea salt and dust, or from anthropogenic emissions, e.g. sulfate and black carbon. On average, anthropogenic aerosol forcing is negative with an effective radiative forcing of -1.6 to $-0.6\,\mathrm{W\,m^{-2}}$ (Bellouin et al. 2020), leading to surface cooling, especially due to sulfate aerosols (Kalisoras et al. 2024). Therefore, a reduction in aerosol concentrations decreases the negative forcing, resulting in surface warming. Anthropogenic aerosol emissions have changed dramatically over the past 100 years. Globally, negative aerosol forcing peaked in the 1980s (Bauer et al. 2022). Since at least 2000, aerosol forcing has become less negative, partly unmasking GHG-induced global warming (Quaas et al. 2022). Because aerosols typically remain in the troposphere for only up to a few days, their direct climate effects are mostly regional. Globally, aerosol effects are spatially heterogeneous because regional aerosol forcing can also induce large remote responses. There are regionally different trends in aerosol emissions and concentrations. Anthropogenic aerosol emissions were strongest in North America and Europe in the late 1970s/1980s (Marmer et al. 2007, Leibensperger et al. 2012, Bauer et al. 2022). Afterwards, they decreased rapidly in those regions while they increased in regions such as South Asia and East Asia (Wang et al. 2015). While emissions started to decrease in East Asia in the early 2010s (Van Der A et al. 2017), they are still increasing in South Asia (Samset et al. 2019). Regions with high levels of air pollution may pursue efforts to improve air quality in the near future, similar to the reductions that began in the US and Europe in the late 1970s/1980s and in China in the early 2010s. Such reductions would improve air quality in regions with currently high air pollution, e.g. South Asia, but would also reduce aerosol-induced cooling and thereby unmask part of the GHG-induced warming. Aerosols also show a clear influence on simulated heat extremes. Aerosol reductions can affect extreme temperatures particularly strongly (Samset et al. 2018), including through both local and remote responses to aerosol changes (Westervelt et al. 2020). Aerosol reductions could also increase the regional warming rate. The potentially increased warming rate could then result in a higher probability of record-breaking heat extremes.

Studies have shown that a higher warming rate leads to more record-breaking heat extremes (Wergen & Krug 2010, Rahmstorf & Coumou 2011, Fischer et al. 2025) and that reductions in aerosol emissions lead to stronger warming (Hodnebrog et al. 2024, Persad et al. 2025, Samset et al. 2025). Yet, it remains unclear (1) whether the effect of changing aerosol concentrations had a significant and detectable effect on observed heat records, and (2) to what extent this aerosol-induced warming amplification may increase the probability of record-breaking heat extremes in the present and near future. In this work, we evaluate whether aerosol reductions lead to a higher probability of record-breaking heat extremes. To do that, we use idealized simulations, single-forcing large ensemble simulations, future regional aerosol scenario simulations, and reanalysis data.

2 Data and Methods

2.1 Data

2.1.1 Idealized simulations First, we created an artificial dataset following idealized forcing scenarios. We generated $k = 1\,000\,000$ simulations of length $n = 200$ years, covering 1850–2050, that follow a non-stationary Generalized Extreme Value (GEV) distribution with typical and non-varying scale ($\sigma = 1.25$) and shape ($\xi = -0.23$) parameter values for a mid-latitude region. The location parameter shifts according to the different forced responses in the scenarios. The scenarios are constant forcing; linear forcing with a 0.5°C increase per decade; constant-then-linear

forcing with constant forcing until 2000 and linear forcing afterwards; linear-then-constant forcing with linear forcing until 2000 and constant forcing afterwards; and trend reversal, which resembles a simplified European forcing trajectory with constant forcing until 1950, followed by negative linear forcing until 1980 and stronger positive linear forcing afterwards (see Figure 1a). The trend reversal and constant-then-linear scenarios are designed to reach the same absolute warming in 2050.

2.1.2 CESM2 large ensemble and single-forcing large ensemble In the second part of our analysis, we used the Community Earth System Model 2 (CESM2) large ensemble (LE) (Rodgers et al. 2021) and single-forcing large ensemble (SFLE) (Simpson et al. 2023) simulations. The LE simulations consist of 100 ensemble members running from 1850 to 2100. They follow historical forcings until 2014 and the Shared Socioeconomic Pathway SSP3-7.0 from 2015 onward. The SSP3-7.0 scenario is characterized by relatively high aerosol loads compared to the other SSPs (Lund et al. 2019). Therefore, the total cooling effect of aerosols is greater than in the other SSPs and shows almost no trend in the first half of the 21st century, whereas in the other scenarios, there is a moderate to strong reducing trend. Given recent global reductions in aerosol concentrations, a reducing trend in the first half of the 21st century seems to be more realistic than no trend (Wang et al. 2021). In the CESM2 SFLE, the simulations run from 1850 to 2050 and follow SSP3-7.0 from 2015 onward. In the SFLE, each experiment simulates changes in only one forcing, while all other forcings are kept constant at pre-industrial levels. In our analysis, we used the greenhouse gas (GHG)-only (15 ensemble members), anthropogenic aerosol (AER)-only (20 ensemble members), biomass burning (BMB)-only (15 ensemble members), and the so-called 'everything-else' (EE; 15 ensemble members) simulations. We analyzed CESM2 heat extremes globally at the grid-cell level and additionally for selected land regions of interest. The regions are Central Europe (CEU; 48°–55°N, 2°–16°E), the Yangtze-Huaihe River Basin in East China (EAC; 26°–34°N, 110°–122°E), and the Eastern Indo-Gangetic Plain in South Asia (IGP; 20°–27°N, 80°–90°E), as examples of regions with diverging aerosol trends. The results are similar for larger regions, suggesting that the conclusions do not depend strongly on the exact box size.

2.1.3 ERA5 and MERRA-2 reanalysis data We used reanalysis data to evaluate the link between changes in aerosol concentrations and the annual record-breaking heat probabilities. The temperature data were derived from ERA5 for 1940–2025. As an indicator of changes in anthropogenic aerosols, we used sulfate aerosol optical depth (SO_4AOD) from the Modern-Era Retrospective analysis for Research and Applications, Version 2 (MERRA-2) for 1980–2025. In MERRA-2, aerosols are simulated with the GEOS-5/GOCART aerosol module and constrained by assimilating bias-corrected AOD from MODIS, AVHRR, and MISR satellite measurements, as well as ground-based AERONET measurements (Randles et al. 2017). We focused on SO_4AOD instead of total AOD because it better isolates anthropogenic sulfate aerosol trends from variability in other aerosol types.

2.1.4 RAMIP simulations To evaluate the effects of future aerosol trends on the annual probability of record-breaking heat extremes in more detail, we used simulations from the Regional Aerosol Model Intercomparison Project (RAMIP; Wilcox et al. (2023)). In these simulations, which run from 2015 to 2050, all forcings except anthropogenic aerosol emissions follow the SSP3-7.0 scenario. Aerosol emissions follow the SSP1-2.6 scenario either globally (SSP370-126aer) or regionally. In the SSP1-2.6 scenario, aerosol concentrations decrease more rapidly globally than in the SSP3-7.0 scenario (Rao et al. 2017, Lund et al. 2019, Wilcox et al. 2023). SSP3-7.0 shows the highest anthropogenic aerosol emissions, whereas SSP1-2.6 shows a rapid decline. The contrast between SSP3-7.0 and SSP1-2.6 could therefore be interpreted as a range of possible future aerosol emissions mitigation pathways. In the regional scenarios, aerosol emissions follow SSP1-2.6 in North America and Europe (SSP370-NAE126aer), East Asia (SSP370-EAS126aer), South Asia (SSP370-SAS126aer), or Africa and the Middle East (SSP370-AFR126aer), and SSP3-7.0 everywhere else. Here, we focused on SSP370-126aer, SSP370-NAE126aer, SSP370-EAS126aer, and SSP370-SAS126aer. Comparing the aerosol scenario simulations to the SSP3-7.0 reference scenario isolates the influence of changes in anthropogenic aerosol levels. SSP370-126aer and the regional perturbations SSP370-EAS126aer, SSP370-NAE126aer and SSP370-SAS126aer all yield significant global-mean effective radiative forcings (ERF; Allen et al. (2026)). More relevant for regional heat extremes, the regional perturbations produce substantially larger ERFs within the perturbed regions, with $1.64 \pm 1.36\,\mathrm{W\,m^{-2}}$ for SSP370-EAS126aer over East Asia, $0.74 \pm 0.21\,\mathrm{W\,m^{-2}}$ for SSP370-NAE126aer over North America and Europe, and $1.61 \pm 1.00\,\mathrm{W\,m^{-2}}$ for SSP370-SAS126aer over South Asia (Allen et al. 2026). These large regional forcings indicate that

regional aerosol perturbations can drive substantial regional temperature responses. We used ten CMIP6 generation models that participated in RAMIP and produced up to 10 realizations for each scenario (see Supplementary Table 1 for more details). The models are CanESM5-1, CESM2, CNRM-ESM2-1, EC-Earth3-AerChem, GFDL-SPEAR_LO, GISS-E2-1-G, MIROC6, MRI-ESM2-0, NorESM2-LM, and UKESM1-0-LL.

2.2 Methods

2.2.1 Definition of record-breaking heat extremes We defined record-breaking heat extremes as new hottest 7-day periods in the historical record, representing persistent and potentially high-impact record heatwaves. For model simulations, we took the hottest 7-day period of daily maximum temperatures (TX7d) for each year as the annual block maximum, following Fischer et al. (2021). Although aerosol effects on solar radiation are particularly relevant for daytime maximum temperatures, the results are similar when using daily mean temperatures, suggesting that the conclusions do not depend strongly on the exact metric. For the reanalysis, we derived the hottest 7-day period for every year from daily mean temperatures (TM7d), because they are more robust than daily maximum temperatures derived from hourly ERA5 data, which may miss the exact daily peak. For the idealized simulations, CESM2 LE and SFLE, and ERA5, we used the previous 50-year period, which implies that 'records' are defined relative to the preceding 50 years only. By using the previous 50-year period instead of the whole historical record, we account for 'forgetting' heat records that occurred a long time ago. When using a 50-year period, the baseline annual record-breaking probability in a stationary climate without a trend in the forced response is around 2% independent of the statistical distribution (Glick 1978, Fischer et al. 2025). For RAMIP, records are defined relative to the full available simulated period starting in 2015 because the simulations are too short for a 50-year reference period.

2.2.2 Annual record-breaking probability In a stationary climate without a trend in the forced response, the annual probability of record-breaking heat extremes would be $1/n$, with n being the number of years in the historical record (Glick 1978). In a non-stationary climate with a linear warming trend in the forced response, the annual probability of record-breaking heat extremes converges to a non-zero constant. In a large ensemble, the annual probability can be derived empirically by counting how many members of the ensemble break a temperature record in a given year. Additionally, the probability can be estimated analytically from the forced response and the variability of the time series. We estimated annual record-breaking probabilities analytically following the record statistics framework of Rahmstorf & Coumou (2011) and Fischer et al. (2021). The probability that the temperature (T) in a given year t_n exceeds all previous years is

$$P_{\mathrm{rec}}(t_n) = \int_{-\infty}^{\infty} f(T, t_n) \prod_{i=1}^{n-1} F(T, t_i)\, \partial T \tag{1}$$

where $f(T, t_n)$ is the probability density function of temperature in the current year t_n, and $\prod_{i=1}^{n-1} F(T, t_i)$ gives the probability that the temperature of that year has not been exceeded before. In most analyses, we compared each year only with the previous 50 years. For a Gaussian distribution with a non-stationary forced response μ_{t_i} and constant standard deviation σ, the probability of setting a new temperature record is

$$P_{\mathrm{rec}}(t_n) = \int_{-\infty}^{\infty} \left[\frac{1}{\sqrt{2\pi\sigma^2}} e^{-\frac{(T-\mu_{t_n})^2}{2\sigma^2}} \right] \prod_{i=1}^{n-1} \left(\frac{1}{2} + \frac{1}{2} \mathrm{erf}\left(\frac{T-\mu_{t_i}}{\sigma\sqrt{2}} \right) \right) \partial T \tag{2}$$

Thus, for warming, the annual probability depends on the number of years in the historical record, the linear trend in the forced response, and the standard deviation of the temperature distribution. Any deviation from the $1/n$ annual probability would indicate a non-stationary climate. Assuming a similar regional forced response trend, the annual probability of record-breaking heat extremes would be higher in tropical regions with lower variability than at mid- and high latitudes, consistent with studies of the signal-to-noise ratio under climate change (Mahlstein et al. 2011). This effect can only be partially offset by the stronger warming trend at high latitudes. Generally, previous records are usually exceeded only by a small absolute margin for narrow distributions.

2.2.3 Preprocessing of model simulations We analyzed heat extremes globally on a grid-cell level and additionally looked at selected land regions of interest. For these regions, we took the spatial mean before calculating TX7d. For the RAMIP simulations, we calculated record-breaking heat

probability anomalies for the period 2041–2050 relative to the SSP3-7.0 reference scenario. We focused on 2041–2050 because the difference between aerosol scenarios is largest toward the end of the RAMIP simulation period. For each RAMIP model, we computed the model ensemble mean before computing the multi-model mean. We estimated uncertainty in the RAMIP multi-model mean by using nonparametric bootstrapping across models. We resampled the 2041–2050 mean probability anomalies of the different models with replacement and show the 2.5th and 97.5th percentiles for the selected regions. For the CESM2 LE and SFLE, we used a 31-year smoothing window for the estimated annual record-breaking probability, whereas for the idealized simulations we did not apply smoothing due to the large sample size.

2.2.4 Reanalysis analysis For the reanalysis, we used TM7d and SO_4AOD for each 5°× 5° land region with a land fraction greater than 50%. Both variables were averaged over these 5°× 5° regions. We focused on land regions and excluded ocean regions because they have different record characteristics. We only considered land regions with a time-mean SO_4AOD greater than 0.1 over the full period 1980–2025 to identify regions with substantial sulfate aerosol influence. This resulted in 125 eligible regions. We computed the change in SO_4AOD from 1980–2009 to 2010–2025. The SO_4AOD change was used as an indicator of the anthropogenic aerosol forcing trend. We then counted the number of record-breaking events for each region from 2010 to 2025. Next, we subtracted the latitudinal average number of record-breaking events to account for the lower internal variability at lower latitudes. By accounting for this covariate, the aerosol signal becomes more pronounced.

3 Results

We first use idealized simulations to illustrate how changes in warming rate affect annual record-breaking probabilities (Section 3.1). We then analyze CESM2 LE and SFLE simulations to assess how different forcings have changed record-breaking probabilities (Section 3.2). We test whether the link between changes in aerosol concentration and the probability of record-breaking heat extremes is detectable in ERA5 and MERRA-2 reanalysis data (Section 3.3). Finally, we assess the impact of future aerosol trends using RAMIP simulations with different aerosol pathways (Section 3.4).

3.1 Record-breaking probabilities in idealized simulations

First, we show the link between a higher warming rate and a higher annual probability of record-breaking heat extremes (Figure 1). The idealized simulations follow non-stationary Generalized Extreme Value (GEV) distributions with a shifting location parameter that changes according to the scenario (see Section 2.1.1). In a stationary climate without warming, the annual

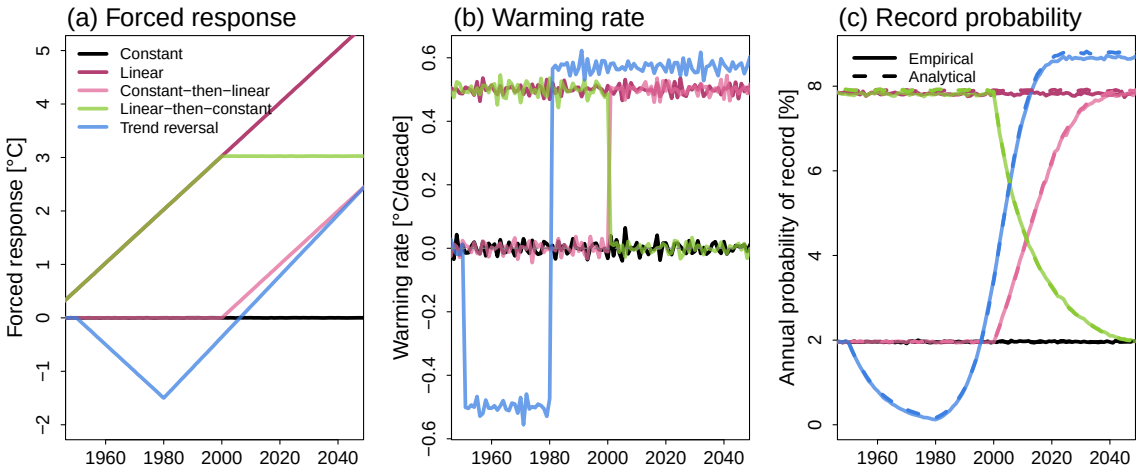

Figure 1. Artificial simulations of idealized scenarios with different forced responses (a), their warming rate (b), and the annual probability of a record-breaking heat extreme relative to the previous 50-year period (c). The solid line shows the empirically derived estimate and the dotted line shows the analytical estimate (see Equation 1) of the annual probability of record-breaking events. The figure is inspired by (Fischer et al. 2021).

probability of hitting a new record that exceeds the maximum of the previous 50 years is constant

at around 2%, as expected from the $1/n$ relation over a sample size of $n = 50$ years. In the case of linear warming throughout the entire period, with a fixed warming rate of 0.5°C/decade, the annual probability of record-breaking heat extremes is constant at around 8%. In scenarios where the warming rate changes within the period, so do the annual record probabilities. In the scenario with a stationary climate until 2000 and linear warming afterwards, the annual record-breaking probability increases from the expected 2% up to 8% within about 20 years. The opposite occurs for a scenario with linear warming followed by a constant forced response. Beyond these changes, the annual record-breaking probability responds with a time lag to changes in the warming rate. After a change in warming rate, record probabilities adjust gradually to the new state. For example, the warming rates of the constant-then-linear and linear-then-constant scenarios intersect in 2000, while their annual record-breaking probabilities intersect only in 2011. This lag of the record probabilities to changes in the warming rate is expected because record probabilities increase (decrease) only gradually after warming accelerates (decelerates), since existing records still reflect the earlier history of warming. Additionally, we consider a trend reversal scenario with cooling from 1950 to 1980, followed by stronger warming than in the other scenarios. This resembles the temperature trend in Europe in a simplified way. In Europe aerosol reductions contributed to additional warming after the 1980s (Glantz et al. 2022). At the end of the study period, the trend reversal scenario reaches the same total warming as the constant-then-linear scenario. However, its annual probability of a new record is consistently higher than that in the constant-then-linear scenario since the 1990s. This illustrates the effect of additional warming after a cooling period, leading to a higher warming rate and thus to more record-breaking events. The effect is similar when using the full simulated record rather than only the preceding 50 years to define record-breaking events.

3.2 Single-forcing large ensemble simulations

Next, we assess how record-breaking probabilities change in CESM2 LE and SFLE simulations. We analyze the temporal evolution of the different forcings in three regions within Europe, East Asia, and South Asia (Figure 2). The forced responses vary substantially between the different scenarios. However, all scenarios show that GHGs are the main driver of regional warming. In all three regions, the GHG-driven forced response increases fairly steadily, whereas the all-forcing LE usually decreases before increasing substantially. The decrease originates from the negative anthropogenic aerosol forcing, whose timing depends on the region.

In Central Europe (CEU), the negative anthropogenic aerosol forcing is strongest around 1980 and weakens afterwards. This leads to a faster increase in the forced response in the all-forcing LE than in GHG-only, as can be seen in the corresponding warming rates. The higher warming rate in the LE compared to GHG-only leads to a considerably higher annual probability of record-breaking heat extremes in CEU in the LE than in GHG-only from around 2000 onward. This means that forcings other than GHGs, namely anthropogenic aerosols, amplify the probability of record-breaking heat extremes. In CEU, the annual probability in the 2020s and 2030s was amplified by 72% in the empirical estimate and by 67% in the analytical estimate.

In East China (EAC), anthropogenic aerosol forcing in CESM2 under SSP3-7.0 reaches a plateau from 2000 to 2040 after strengthening until around 2000. In this scenario, the warming rates of the all-forcing LE and GHG-only are fairly similar in that period. In that case, the annual record-breaking probabilities of the LE and GHG-only become similar around 2020. Note that in reality anthropogenic aerosols started to decrease as early as in the 2010s in China (Van Der A et al. 2017). Assuming a continued trend of aerosol reduction in EAC, the warming rate and thus the annual record-breaking probability would increase even more due to the relative positive anthropogenic aerosol forcing from aerosol reduction.

In the Indo-Gangetic Plain in South Asia (IGP), the negative anthropogenic aerosol forced response is strongest among the three regions and continues to increase in magnitude until the mid to late 2030s in the SSP3-7.0 scenario. Since the negative anthropogenic aerosol forcing has a similar magnitude as the positive GHG forcing, there is only a small forced response in the LE. It only emerges by the late 2030s, when anthropogenic aerosol forcing starts to plateau. Therefore, the record-breaking probabilities are substantially higher in the GHG-only simulations than in the LE up until the 2030s. In the 2020s, mainly aerosols damp the annual record-breaking probability on average by 28% for the empirical and by 47% for the analytical estimate. Close to the end of the simulations, the probability in the LE catches up to the probability in GHG-only.

As an illustrative example of current climate conditions, we use the year 2026 to evaluate where the probability of record-breaking heat extremes is higher or lower in the all-forcing LE than in the GHG-only simulations in CESM2, using analytically derived probabilities (Figure 3). The results

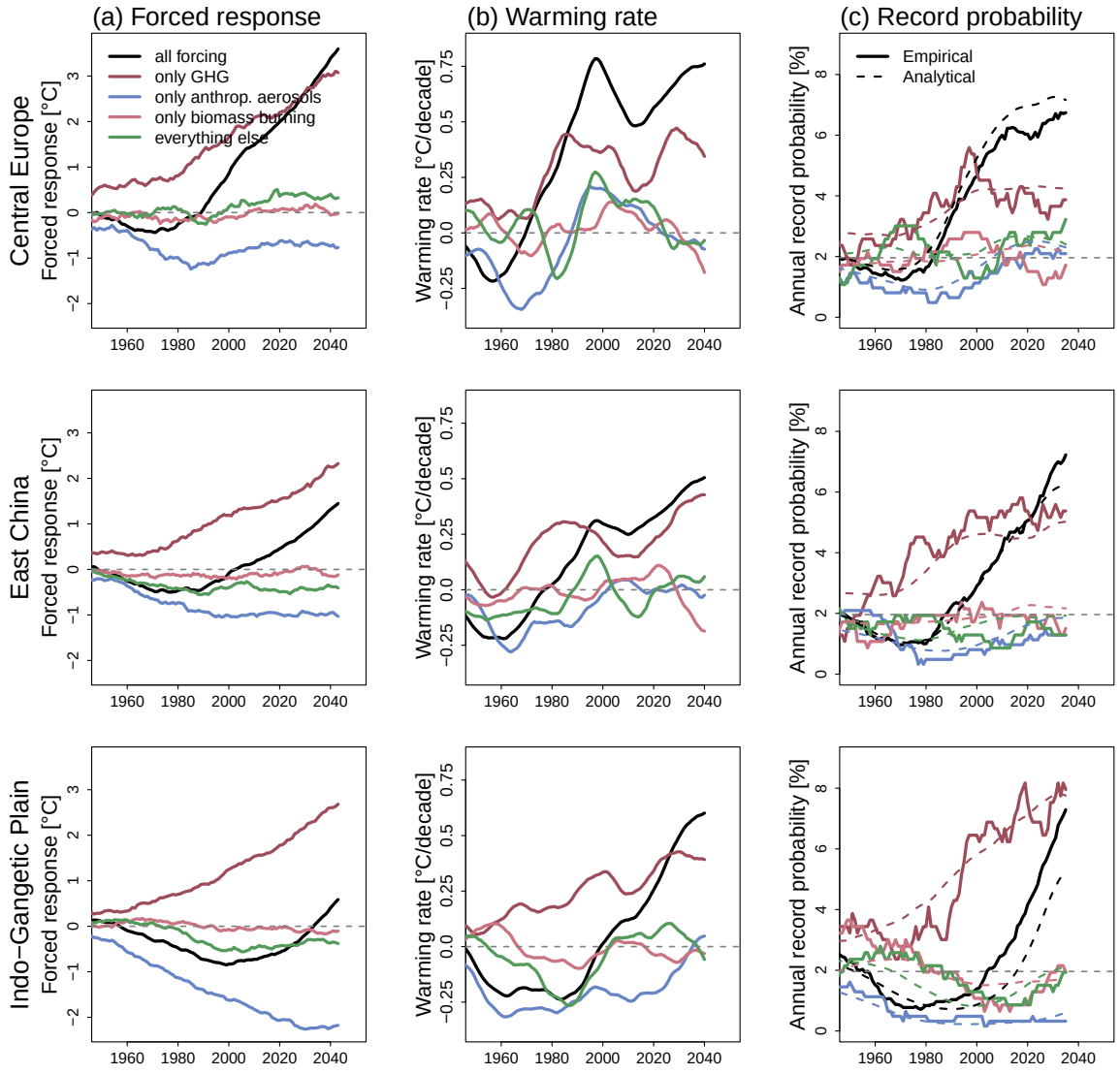

Figure 2. The temporal evolution of the hottest 7-day period of daily maximum temperatures (TX7d) is illustrated for three selected regions in the CESM2 large ensemble and single-forcing large ensemble simulations. Columns show (a) the 15-year smoothed averaged forced response of TX7d, (b) the warming rate in the forced response using a 21-year sliding linear trend, and (c) the 31-year smoothed annual probability of a record-breaking heat extreme relative to the previous 50-year period. The three rows show Central Europe, East China, and the eastern Indo-Gangetic Plain in South Asia, respectively. The solid lines show the empirically derived estimate and the dotted lines show the analytical estimate of the annual probability of record-breaking events.

are similar when deriving the annual record-breaking probabilities empirically which have more noise (Supplementary Figure 1). In regions where the probability is higher in the LE, indicated by red colors, other forcings, especially decreasing anthropogenic aerosols, amplify the probability of record-breaking heat extremes. Most parts of the Northern Hemisphere continents show a positive ratio, meaning that the probability is amplified by forcings other than GHGs. The magnitude of the amplification is substantial, exceeding 50% in many parts of Europe and North America. Thus, forcings that cause a smaller absolute temperature response than GHGs can still strongly affect the annual record-breaking probability if they substantially change the regional warming rate. Irrespective of the derivation method, South Asia stands out as the region where the annual probability of record-breaking heat extremes is most clearly lower in the LE than in GHG-only, with differences exceeding 20% across most of the region. Parts of Africa, especially West Africa, also show lower probabilities but with a smaller difference between the LE and GHG-only. This is consistent with ongoing increases in aerosol forcing in South Asia (Samset et al. 2019) and projected increases in African aerosol emissions in several scenarios (Amooli et al. 2025).

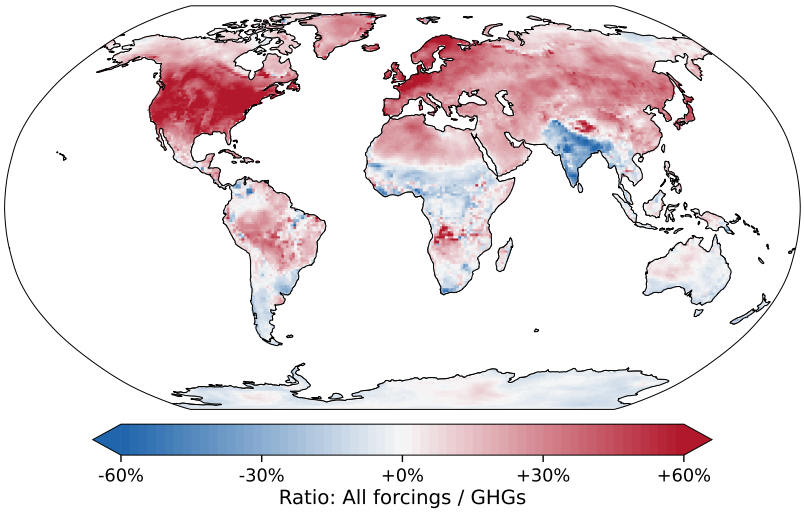

Figure 3. Ratio between the 31-year smoothed analytically derived annual record-breaking probability in the CESM2 large ensemble and the GHG-only simulations from the CESM2 single-forcing large ensemble for each grid point for the year 2026. Mid-latitude regions of North America, Europe and East Asia stick out as hotspot regions of elevated risk of heat records due to reduced aerosol forcing.

3.3 Detecting changes in heat extremes due to aerosol forcing in reanalysis data

In reanalysis data, we test whether changes in aerosol concentrations are linked to changes in the probability of record-breaking heat extremes. Before relating record probabilities to SO_4AOD changes, we account for the latitudinal dependence of record-breaking heat extremes (Supplementary Figure 2), which could act as a covariate. Although the latitudinal mean can itself be influenced by strong regional aerosol trends, subtracting it allows us to separate regional signals from the broader latitude effect. In ERA5, record-breaking heat extremes occur more frequently at low latitudes and less frequently at mid-latitudes, in line with the earlier emergence of significant warming in low-latitude regions (Mahlstein et al. 2011). At Northern Hemisphere high latitudes, the probability increases again due to Arctic amplification. The higher annual probability at low latitudes originates from lower inter-annual variability, which results in a narrower TM7d distribution. At mid-latitudes, the TM7d distribution is broader, resulting in fewer record-breaking heat extremes. However, when they occur, records at mid-latitudes can exceed previous records by a larger absolute margin when compared to records at low latitudes.

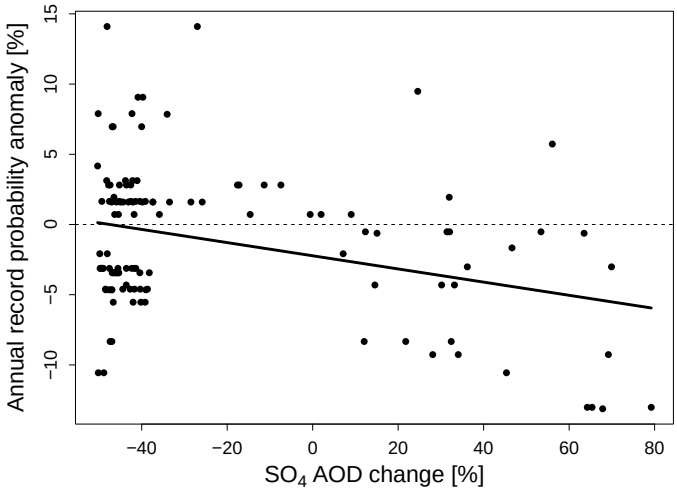

Figure 4. Annual probability anomaly of hottest 7-day period of daily mean temperature (TM7d) records in reanalysis data with respect to the latitudinal mean annual record probability from 2010 to 2025 versus the change in sulfate aerosol optical depth (SO_4AOD) from 1980–2009 to 2010–2025 for $5° \times 5°$ land regions where over the period 1980–2025 the average $SO_4\text{AOD} > 0.1$. Records are defined relative to the maximum in the preceding 50-year period. The black line shows the linear regression, with a statistically significant slope of -0.5 percentage points in annual record probability anomaly per 10% change in SO_4AOD.

After accounting for these latitudinal differences, we test whether changes in aerosol concentrations further modulate the probability of record events. We show the link between changes in SO_4AOD in recent decades and the annual record-breaking probability anomaly with respect to the latitudinal mean in the period 2010–2025 (Figure 4). The annual record-breaking probability anomaly decreases with increasing SO_4AOD. The linear regression slope is statistically significant ($p = 0.0002$), showing that a 10% decrease in SO_4AOD is associated with a 0.5 percentage points higher annual probability of record-breaking heat extremes. Considering that the global land-mean record-breaking heat probability in the period 2010–2025 is $P = 6.7\%$, a change of 0.5 percentage points per 10% change in SO_4AOD is substantial. Additionally, there are almost no regions with a positive annual record-breaking probability anomaly when SO_4AOD increased by more than 40%.

We also tested total AOD instead of SO_4AOD using the same approach, except that the threshold for regional mean AOD was set to 0.2 instead of 0.1 to account for the higher overall AOD. Using total AOD, we also find a statistically significant slope ($p = 0.01$) of -0.6 percentage points in annual record probability anomaly per 10% change in AOD (Supplementary Figure 3). Thus, the slope is similar for SO_4AOD and total AOD. Compared to SO_4AOD, total AOD shows stronger variability, as expected because SO_4AOD better isolates the anthropogenic sulfate aerosol signal, whereas total AOD includes other aerosol types such as dust and sea salt that have natural variability.

3.4 RAMIP simulations

Finally, we assess how annual record-breaking heat probabilities change under different near-term future aerosol scenarios using RAMIP simulations for 2041–2050. These experiments isolate the effects of aerosol emission changes by comparing scenarios with different global or regional aerosol reductions while keeping all other forcings identical. Here, we show the analytically derived annual probability of record-breaking heat extremes, calculated from the forced response and the variability of the SSP3-7.0 and RAMIP simulations. We assess SSP3-7.0 and anomalies relative to SSP3-7.0 for four RAMIP scenarios, namely global aerosol reduction to SSP1-2.6 and three regional aerosol reduction scenarios in North America and Europe, East Asia, and South Asia, for the period 2041–2050 (Figure 5). The empirically derived annual probability for the RAMIP scenarios is shown in Supplementary Figure 4. Overall, both methods show similar regional patterns, but the empirically derived probabilities are more heterogeneous and regionally less robust than the analytical estimates. In the SSP3-7.0 baseline scenario, the expected global spatial structure of record-breaking heat extremes emerges. In regions with smaller inter-annual variability, the probability of setting new temperature records in a warming world increases. Thus, low-latitude regions show the highest annual record-breaking probabilities. More relevant for this study is how these record-breaking probabilities change in different aerosol scenarios. First, we look at global aerosol reduction, where anthropogenic aerosols follow the SSP1-2.6 scenario globally, while all other forcings follow SSP3-7.0 (SSP370-126aer). In SSP370-126aer, most land regions, especially in the Northern Hemisphere, experience more frequent temperature records than in SSP3-7.0. Most models agree on the sign of change. The annual record-breaking probabilities are amplified by reducing aerosol concentrations by up to 5 percentage points regionally. When aerosols are reduced only regionally, the global signal in record-breaking probability anomalies is substantially smaller than in SSP370-126aer, consistent with the smaller global-mean ERF of the regional perturbations (Allen et al. 2026). Nevertheless, the regional perturbations still affect record-breaking probabilities in the perturbed regions and in some remote regions. The responses in the perturbed regions are generally smaller than for global aerosol reductions, in line with the substantial contribution of remote aerosol reductions to the regional ERF in SSP370-126aer (Allen et al. 2026).
SSP370-NAE126aer results in a higher annual record-breaking probability in the central US and eastern Europe. However, the changes are rather small and robust in only a few regions. In North America and Europe, aerosols have already decreased in recent decades, and the absolute changes possible in the 2040s by reducing aerosol emissions from SSP3-7.0 to SSP1-2.6 are limited. In SSP370-EAS126aer, a robust signal is detected in East Asia, where the probability of new temperature records increases. The strongest regional effect occurs in SSP370-SAS126aer. In this scenario, the RAMIP models agree that reducing regional aerosol emissions to SSP1-2.6 levels clearly increases the annual record-breaking probability in South Asia and Southeast Asia. All regional aerosol reductions also show some remote effects outside the perturbed regions.

In the three selected regions, Central Europe (CEU), East China (EAC), and the Eastern Indo-Gangetic Plain (IGP), the effects of aerosol reductions vary in the 2040s. All three regions have similar annual record-breaking probabilities in the SSP3-7.0 baseline scenario with 7.2%, 8.8%, and 6.7% in CEU, EAC, and IGP, respectively. The individual model anomalies in the

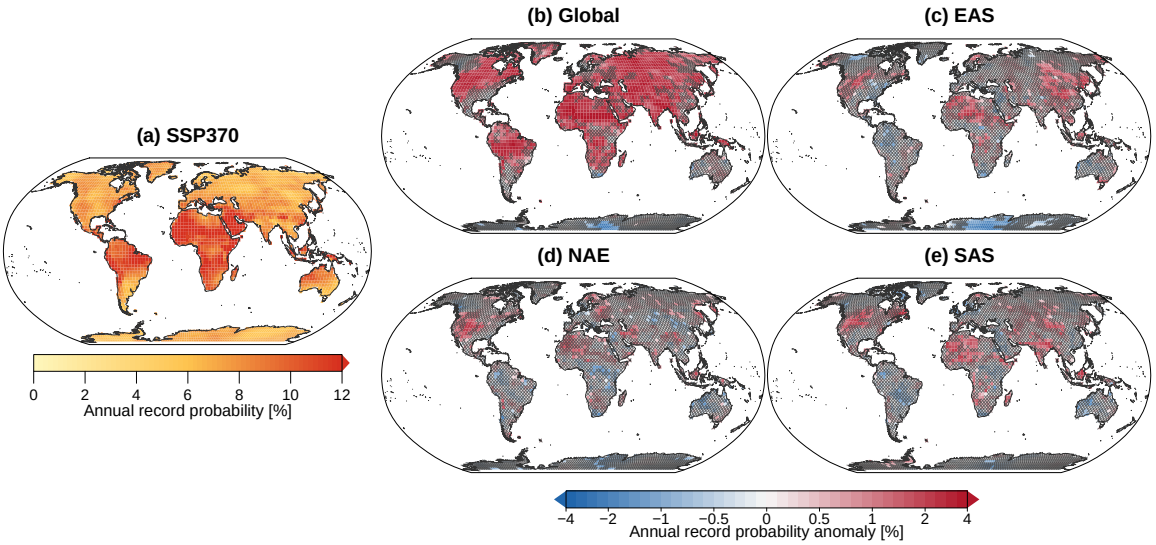

Figure 5. Annual probability of analytically derived record-breaking heat extremes of hottest 7-day period of daily maximum temperatures (TX7d) in the Regional Aerosol Model Intercomparison Project (RAMIP) for the period 2041–2050, with records defined relative to the preceding annual maxima since 2015 within each simulation. (a) Absolute annual record-breaking heat probability in the SSP3-7.0 reference scenario. (b)–(e) Annual record-breaking heat probability anomaly with respect to SSP3-7.0 for different RAMIP scenarios, where anthropogenic aerosols follow the SSP1-2.6 scenario either globally or only in selected regions, namely North America and Europe (NAE), East Asia (EAS), and South Asia (SAS). Hatching indicates grid cells where fewer than 8 out of the 10 models agree on the sign of change as a measure of robustness.

different aerosol scenarios within RAMIP are shown in Supplementary Table 2. In the multi-model mean, the global aerosol reduction in SSP370-126aer leads to a 4.7 [95% bootstrap interval: 3.4, 5.9] percentage points increase in annual record-breaking heat probability in IGP in the 2040s when estimating the probabilities analytically. This means that the annual record-breaking probability increases from 6.7% in SSP3-7.0 to 11.4% in SSP370-126aer. All 10 models agree on the positive sign, indicating a robust positive signal. When deriving the probabilities empirically, the values are slightly higher with a 5.8 [3.7, 7.6] percentage points increase. SSP370-126aer leads to smaller changes in the other regions where record-breaking probabilities increase by 0.4 [−1.7, 2.0] percentage points and 0.8 [−0.6, 2.2] percentage points in EAC and CEU, respectively, in the analytical estimate and by 1.1 [−1.7, 3.6] percentage points and 1.2 [−1.5, 4.2] percentage points in the empirical estimate. In EAC, 8 out of 10 models agree on a positive sign, but one model shows a strongly negative response, reducing the multi-model mean. For the selected regions, we next analyze the effects of the corresponding larger regional aerosol reductions. SSP370-SAS126aer leads to 1.7 [0.5, 2.9] percentage points higher annual record probabilities in IGP than in SSP3-7.0 in the analytical estimate, with 8 out of 10 models agreeing on the sign. The empirical estimate shows a larger increase of 3.1 [0.9, 5.5] percentage points. SSP370-EAS126aer leads to 0.6 [−1.6, 2.5] percentage points higher annual record probabilities in EAC than in SSP3-7.0 in the analytical estimate. Seven out of 10 models agree on the positive sign, but one model shows a strongly negative response and thereby reduces the multi-model mean. The empirical estimate shows a larger increase of 1.5 [−2.1, 5.1] percentage points. SSP370-NAE126aer leads to almost no change in annual record probabilities in CEU compared with SSP3-7.0. Most models show only small changes (less than ±1 percentage point), and they disagree on the sign. The effect of SSP370-NAE126aer is larger in eastern Europe than in the selected CEU region.

4 Discussion and Conclusion

We show that regional anthropogenic aerosol trends modulate the annual probability of record-breaking heat extremes. The link between aerosol trends and record probability is conceptually clear: decreasing regional aerosol emissions can contribute to a higher warming rate. The higher the warming rate, the higher the probability of record-breaking heat extremes (Section 3.1). In the CESM2 LE and SFLE, differences between the all-forcing LE and the GHG-only simulations arise in regions with strong aerosol trends (Section 3.2). Regions where aerosol forcing is decreasing in strength, such as Europe and North America, show higher annual probabilities of record-breaking heat extremes in the all-forcing LE than in the GHG-only simulations. Thus, the record probabilities are amplified by forcings other than GHGs. Based on the SFLE and RAMIP

results, we argue that this amplification is mainly driven by anthropogenic aerosol trends. In reanalysis data, we find a statistically significant relationship between changes in aerosol concentrations and the probability of record-breaking heat extremes (Section 4). This indicates that regions where aerosol concentrations increased had fewer record exceedances than regions where aerosol concentrations decreased. The RAMIP simulations show that lower future aerosol emissions increase record-breaking heat probabilities in the 2040s relative to SSP3-7.0 (Section 3.4). The strongest response occurs for global aerosol reductions in SSP370-126aer, with substantial and robust increases over large parts of the globe. Regional aerosol reductions produce smaller but still relevant responses. They cause robust increases in parts of the target regions, especially for the South Asian perturbation, where aerosol concentrations remain high and their reduction can lead to substantial additional warming. The East Asian perturbation also shows a regional increase, although the multi-model mean is reduced by one model with a strongly negative response. The North America and Europe perturbation produces less robust changes, consistent with the smaller difference in aerosol emissions between SSP1-2.6 and SSP3-7.0 in the mid-21st century (Wilcox et al. 2023). The regional perturbations also produce remote effects, showing that aerosol reductions can affect record-breaking heat probabilities beyond the perturbed region.

Regions where aerosol concentrations have declined in recent decades are at a higher risk of record-breaking heat extremes due to the higher warming rate. The probability could be particularly amplified in regions with a strong and sudden aerosol decline. In China, SO_2 emissions declined sharply by 62% from 2010 to 2017 (Zheng et al. 2018). The additional warming resulting from aerosol reductions in East Asia could even explain the higher global warming rate during 2013–2022 (Samset et al. 2025). The higher global warming rate, and especially the higher regional warming rate in East Asia, is expected to lead to more record-breaking heat extremes. Thus, the aerosol-induced amplification of record-breaking heat extremes in East Asia is expected to be larger than estimated in CESM2 (Figure 3). Additionally, CMIP6 historical simulations underestimate the recent aerosol reductions in East Asia up to 2014 due to the CEDS emissions inventory used for CMIP6 (Wang et al. 2021). This underestimation can extend into near-term projections. Low-emission scenarios such as SSP1-2.6 catch up later (Samset et al. 2025), whereas high-emission scenarios such as SSP3-7.0 continue to miss the observed aerosol decline. Because record-breaking probabilities respond with a time lag to changes in the regional warming rate, the statistical risk increases every year without a record heat extreme when the recent warming rate has been positive. Thus, the most at-risk regions for record-breaking heat extremes are regions where the current record is lower than expected from the forced response and where the warming rate has been amplified in recently. Elevated future probabilities of record-breaking heat extremes can also originate from strong aerosol decreases. This could occur in South Asia if aerosols start to decrease there. Therefore, adaptation measures are especially important when aerosols decline.

Our climate model results attributing parts of the record-breaking heat changes to aerosol reductions are limited by uncertainty in aerosol-cloud interactions. In heavily polluted regions, cloud droplet responses to aerosol changes can saturate, delaying the climate penalty from air quality improvements by two to three decades (Jia & Quaas 2023). This suggests that the timing of aerosol-induced increases in warming rate and record-breaking heat probability may depend on how well models represent this saturation. Additionally, for RAMIP, future work could investigate the mechanisms driving different model responses and use the inter-member spread to assess the role of internal variability relative to forced aerosol-driven changes in record-breaking heat probabilities.

However, the main open question is how regional aerosol trends will evolve in the future. In particular, SSP3-7.0, with its high aerosol emissions, seems unrealistic globally and for regions with strong aerosol reductions, such as East Asia, where it misses the observed sulfate aerosol reduction. Regions such as South Asia and Africa, where aerosol emissions are still increasing, are of particular interest. If aerosol emissions begin to decrease sharply, similar to China in the 2010s, record-breaking heat extremes could increase substantially in the near future.

Despite the evidence that regional aerosol trends modulate the probability of record-breaking heat extremes, increasing GHG concentrations remain the dominant driver of more record heat extremes globally. Aerosol reductions only unmask part of GHG-induced global warming. This unmasking leads to temporarily elevated record-breaking probabilities. Nonetheless, air quality improvements should remain a high priority for human health. Globally, strong reductions of GHG emissions are needed to prevent more record-breaking heat extremes in the long term. Adaptation measures should therefore account for temporary increases in record probability due to aerosol reductions. In this study, we show that changes in regional aerosol concentrations can substantially modulate the probability of record-breaking heat extremes by altering regional warming rates.

Acknowledgments
We acknowledge the efforts of RAMIP modelling centres and data providers, the Centre for Environmental Data Analysis for archiving the data and providing access, and the multiple funding agencies who support RAMIP and CEDA. We acknowledge NCAR and all the scientists, software engineers and administrators who contributed to the development of the Community Earth System Model. We acknowledge the CESM2 Large Ensemble Community Project and supercomputing resources provided by the IBS Center for Climate Physics in South Korea.

Funding
F. K., P. P., and S. S. acknowledge the climXtreme project funded by the German Federal Ministry of Education and Research (Phase 2, project PATTETA, grant number 01LP2323C) and the project 'Artificial Intelligence for Enhanced Representation of Processes and Extremes in Earth System Models' (AI4PEX; grant agreement 101137682, funded by the EU's Horizon Europe program). S. A. acknowledges the University of Reading Advancing the Frontiers of Earth System Prediction (AFESP) Programme [award number A3720200]. G. G. P. acknowledges funding from the U.S. National Oceanic and Atmospheric Administration under award NA23OAR4310601.

Author contributions
Florian Kraulich: Writing – original draft, Writing – review & editing, Visualization, Investigation, Methodology, Formal analysis, Conceptualization. Peter Pfleiderer: Writing – review & editing, Investigation, Methodology, Supervision, Conceptualization. Sharar Ahmadi: Resources, Data curation. Robert J. Allen: Resources, Data curation, Writing – review & editing. Pierre Nabat: Resources, Data curation, Writing – review & editing. Geeta G. Persad: Resources, Data curation, Writing – review & editing. Bjørn H. Samset: Resources, Data curation, Writing – review & editing. Laura J. Wilcox: Resources, Data curation, Writing – review & editing. Sebastian Sippel: Writing – review & editing, Investigation, Methodology, Funding acquisition, Supervision, Conceptualization.

Data availability
The CESM2 LE data used in this study are obtained from https://doi.org/10.26024/kgmp-c556 (Rodgers et al. 2021) and the CESM2 SFLE data from https://doi.org/10.26024/yw4w-1w27 (Simpson et al. 2023). MERRA-2 reanalysis is available from NASA's GES DISC (https://disc.gsfc.nasa.gov/datasets?project=MERRA-2; Gelaro et al. (2017)). ERA5 reanalysis is available from the Copernicus Climate Change Service Climate Data Store (https://doi.org/10.24381/cds.bd0915c6; Hersbach et al. (2020)). RAMIP simulations are made available through CEDA (https://www.ceda.ac.uk/). For access instructions, see https://catalogue.ceda.ac.uk/uuid/4680fd74cf2244ba8476ed2617e3b41f/ .

References
Allen, R. J., Wilcox, L. J., Samset, B. H., Ahmadi, S., Ekman, A. M. L., Elling, M. T., Fraser-Leach, L., Griffiths, P., Keeble, J., Koshiro, T., Kushner, P., Lewinschal, A., MacRae, M., Makkonen, R., Merikanto, J., Nabat, P., Nazarenko, L., O'Donnell, D., Oshima, N., Paynter, D., Persad, G., Rumbold, S. T., Swart, N., Takemura, T., Tsigaridis, K., Von Salzen, K. & Westervelt, D. M. (2026), 'Decomposing the global and regional aerosol effective radiative forcing associated with strong versus weak air quality policies by Mid-21st century', *Environmental Research: Climate* **5**(2), 025014.
URL: *https://iopscience.iop.org/article/10.1088/2752-5295/ae5418*

Amooli, J. A., Lund, M. T., Chowdhury, S., Myhre, G., Johansen, A. N., Samset, B. H. & Westervelt, D. M. (2025), 'An uncertain future for the climate and health impacts of anthropogenic aerosols in Africa', *Atmospheric Chemistry and Physics* **25**(19), 11611–11632.
URL: *https://acp.copernicus.org/articles/25/11611/2025/*

Bauer, S. E., Tsigaridis, K., Faluvegi, G., Nazarenko, L., Miller, R. L., Kelley, M. & Schmidt, G. (2022), 'The Turning Point of the Aerosol Era', *Journal of Advances in Modeling Earth Systems* **14**(12), e2022MS003070.
URL: *https://agupubs.onlinelibrary.wiley.com/doi/10.1029/2022MS003070*

Bellouin, N., Quaas, J., Gryspeerdt, E., Kinne, S., Stier, P., Watson-Parris, D., Boucher, O., Carslaw, K. S., Christensen, M., Daniau, A., Dufresne, J., Feingold, G., Fiedler, S., Forster, P., Gettelman, A., Haywood, J. M., Lohmann, U., Malavelle, F., Mauritsen, T., McCoy, D. T.,

Myhre, G., Mülmenstädt, J., Neubauer, D., Possner, A., Rugenstein, M., Sato, Y., Schulz, M., Schwartz, S. E., Sourdeval, O., Storelvmo, T., Toll, V., Winker, D. & Stevens, B. (2020), 'Bounding Global Aerosol Radiative Forcing of Climate Change', *Reviews of Geophysics* **58**(1), e2019RG000660.
URL: *https://agupubs.onlinelibrary.wiley.com/doi/10.1029/2019RG000660*

Engdaw, M. M., Steiner, A. K., Hegerl, G. C. & Ballinger, A. P. (2023), 'Attribution of observed changes in extreme temperatures to anthropogenic forcing using CMIP6 models', *Weather and Climate Extremes* **39**, 100548.
URL: *https://linkinghub.elsevier.com/retrieve/pii/S2212094723000014*

Fischer, E. M., Bador, M., Huser, R., Kendon, E. J., Robinson, A. & Sippel, S. (2025), 'Record-breaking extremes in a warming climate', *Nature Reviews Earth & Environment* **6**(7), 456–470.
URL: *https://www.nature.com/articles/s43017-025-00681-y*

Fischer, E. M., Sippel, S. & Knutti, R. (2021), 'Increasing probability of record-shattering climate extremes', *Nature Climate Change* **11**(8), 689–695.
URL: *https://www.nature.com/articles/s41558-021-01092-9*

Forster, P. M., Smith, C., Walsh, T., Lamb, W. F., Lamboll, R., Cassou, C., Hauser, M., Hausfather, Z., Lee, J.-Y., Palmer, M. D., Von Schuckmann, K., Slangen, A. B. A., Szopa, S., Trewin, B., Yun, J., Gillett, N. P., Jenkins, S., Matthews, H. D., Raghavan, K., Ribes, A., Rogelj, J., Rosen, D., Zhang, X., Allen, M., Aleluia Reis, L., Andrew, R. M., Betts, R. A., Borger, A., Broersma, J. A., Burgess, S. N., Cheng, L., Friedlingstein, P., Domingues, C. M., Gambarini, M., Gasser, T., Gütschow, J., Ishii, M., Kadow, C., Kennedy, J., Killick, R. E., Krummel, P. B., Liné, A., Monselesan, D. P., Morice, C., Mühle, J., Naik, V., Peters, G. P., Pirani, A., Pongratz, J., Minx, J. C., Rigby, M., Rohde, R., Savita, A., Seneviratne, S. I., Thorne, P., Wells, C., Western, L. M., Van Der Werf, G. R., Wijffels, S. E., Masson-Delmotte, V. & Zhai, P. (2025), 'Indicators of Global Climate Change 2024: annual update of key indicators of the state of the climate system and human influence', *Earth System Science Data* **17**(6), 2641–2680.
URL: *https://essd.copernicus.org/articles/17/2641/2025/*

Gasparrini, A., Guo, Y., Hashizume, M., Lavigne, E., Zanobetti, A., Schwartz, J., Tobias, A., Tong, S., Rocklöv, J., Forsberg, B., Leone, M., De Sario, M., Bell, M. L., Guo, Y.-L. L., Wu, C.-f., Kan, H., Yi, S.-M., De Sousa Zanotti Stagliorio Coelho, M., Saldiva, P. H. N., Honda, Y., Kim, H. & Armstrong, B. (2015), 'Mortality risk attributable to high and low ambient temperature: a multicountry observational study', *The Lancet* **386**(9991), 369–375.
URL: *https://linkinghub.elsevier.com/retrieve/pii/S0140673614621140*

Gelaro, R., McCarty, W., Suárez, M. J., Todling, R., Molod, A., Takacs, L., Randles, C. A., Darmenov, A., Bosilovich, M. G., Reichle, R., Wargan, K., Coy, L., Cullather, R., Draper, C., Akella, S., Buchard, V., Conaty, A., Da Silva, A. M., Gu, W., Kim, G.-K., Koster, R., Lucchesi, R., Merkova, D., Nielsen, J. E., Partyka, G., Pawson, S., Putman, W., Rienecker, M., Schubert, S. D., Sienkiewicz, M. & Zhao, B. (2017), 'The Modern-Era Retrospective Analysis for Research and Applications, Version 2 (MERRA-2)', *Journal of Climate* **30**(14), 5419–5454.
URL: *https://journals.ametsoc.org/doi/10.1175/JCLI-D-16-0758.1*

Glantz, P., Fawole, O. G., Ström, J., Wild, M. & Noone, K. J. (2022), 'Unmasking the Effects of Aerosols on Greenhouse Warming Over Europe', *Journal of Geophysical Research: Atmospheres* **127**(22), e2021JD035889.
URL: *https://agupubs.onlinelibrary.wiley.com/doi/10.1029/2021JD035889*

Glick, N. (1978), 'Breaking records and breaking boards', *The American Mathematical Monthly* **85**(1), 2–26.

Gulev, S. K., Thorne, P. W., Ahn, J., Dentener, F. J., Domingues, C. M., Gerland, S., Gong, D., Kaufman, D. S., Nnamchi, H. C., Quaas, J., Rivera, J. A., Sathyendranath, S., Smith, S. L., Trewin, B., von Schuckmann, K., Vose, R. S., Masson-Delmotte, V., Zhai, P., Pirani, A., Connors, S. L., Péan, C., Berger, S., Caud, N., Chen, Y., Goldfarb, L., Gomis, M. I., Huang, M., Leitzell, K., Lonnoy, E., Matthews, J. B. R., Maycock, T. K., Waterfield, T., Yelekçi, O., Yu, R., Zhou, B. & Gulev (2021), Changing state of the climate system, *in* 'Climate change 2021: The physical science basis. Contribution of working group I to the sixth assessment report of the

intergovernmental panel on climate change', Cambridge University Press, Cambridge, United Kingdom and New York, NY, USA, pp. 287–422.

Hersbach, H., Bell, B., Berrisford, P., Hirahara, S., Horányi, A., Muñoz-Sabater, J., Nicolas, J., Peubey, C., Radu, R., Schepers, D. & others (2020), 'The ERA5 global reanalysis', *Quarterly journal of the royal meteorological society* **146**(730), 1999–2049.

Hodnebrog, O., Myhre, G., Jouan, C., Andrews, T., Forster, P. M., Jia, H., Loeb, N. G., Olivié, D. J. L., Paynter, D., Quaas, J., Raghuraman, S. P. & Schulz, M. (2024), 'Recent reductions in aerosol emissions have increased Earth's energy imbalance', *Communications Earth & Environment* **5**(1), 166.
URL: *https://www.nature.com/articles/s43247-024-01324-8*

Jia, H. & Quaas, J. (2023), 'Nonlinearity of the cloud response postpones climate penalty of mitigating air pollution in polluted regions', *Nature Climate Change* **13**(9), 943–950.
URL: *https://www.nature.com/articles/s41558-023-01775-5*

Kalisoras, A., Georgoulias, A. K., Akritidis, D., Allen, R. J., Naik, V., Kuo, C., Szopa, S., Nabat, P., Olivié, D., Van Noije, T., Le Sager, P., Neubauer, D., Oshima, N., Mulcahy, J., Horowitz, L. W. & Zanis, P. (2024), 'Decomposing the effective radiative forcing of anthropogenic aerosols based on CMIP6 Earth system models', *Atmospheric Chemistry and Physics* **24**(13), 7837–7872.
URL: *https://acp.copernicus.org/articles/24/7837/2024/*

Leibensperger, E. M., Mickley, L. J., Jacob, D. J., Chen, W.-T., Seinfeld, J. H., Nenes, A., Adams, P. J., Streets, D. G., Kumar, N. & Rind, D. (2012), 'Climatic effects of 1950–2050 changes in US anthropogenic aerosols – Part 1: Aerosol trends and radiative forcing', *Atmospheric Chemistry and Physics* **12**(7), 3333–3348.
URL: *https://acp.copernicus.org/articles/12/3333/2012/*

Lund, M. T., Myhre, G. & Samset, B. H. (2019), 'Anthropogenic aerosol forcing under the Shared Socioeconomic Pathways', *Atmospheric Chemistry and Physics* **19**(22), 13827–13839.
URL: *https://acp.copernicus.org/articles/19/13827/2019/*

Mahlstein, I., Knutti, R., Solomon, S. & Portmann, R. W. (2011), 'Early onset of significant local warming in low latitude countries', *Environmental Research Letters* **6**(3), 034009.

Marmer, E., Langmann, B., Fagerli, H. & Vestreng, V. (2007), 'Direct shortwave radiative forcing of sulfate aerosol over Europe from 1900 to 2000', *Journal of Geophysical Research: Atmospheres* **112**(D23), 2006JD008037.
URL: *https://agupubs.onlinelibrary.wiley.com/doi/10.1029/2006JD008037*

Mora, C., Dousset, B., Caldwell, I. R., Powell, F. E., Geronimo, R. C., Bielecki, C., Counsell, C. W. W., Dietrich, B. S., Johnston, E. T., Louis, L. V., Lucas, M. P., McKenzie, M. M., Shea, A. G., Tseng, H., Giambelluca, T. W., Leon, L. R., Hawkins, E. & Trauernicht, C. (2017), 'Global risk of deadly heat', *Nature Climate Change* **7**(7), 501–506.
URL: *https://www.nature.com/articles/nclimate3322*

Perkins-Kirkpatrick, S. E. & Lewis, S. C. (2020), 'Increasing trends in regional heatwaves', *Nature Communications* **11**(1), 3357.
URL: *https://www.nature.com/articles/s41467-020-16970-7*

Persad, G. G., Cummins, C. & Baldwin, J. W. (2025), 'Anthropogenic aerosol changes disproportionately impact the evolution of global heatwave hazard and exposure', *Environmental Research Letters* **20**(8), 084023.
URL: *https://iopscience.iop.org/article/10.1088/1748-9326/addee0*

Quaas, J., Jia, H., Smith, C., Albright, A. L., Aas, W., Bellouin, N., Boucher, O., Doutriaux-Boucher, M., Forster, P. M., Grosvenor, D., Jenkins, S., Klimont, Z., Loeb, N. G., Ma, X., Naik, V., Paulot, F., Stier, P., Wild, M., Myhre, G. & Schulz, M. (2022), 'Robust evidence for reversal of the trend in aerosol effective climate forcing', *Atmospheric Chemistry and Physics* **22**(18), 12221–12239.
URL: *https://acp.copernicus.org/articles/22/12221/2022/*

Rahmstorf, S. & Coumou, D. (2011), 'Increase of extreme events in a warming world', *Proceedings of the National Academy of Sciences* **108**(44), 17905–17909.
URL: *https://pnas.org/doi/full/10.1073/pnas.1101766108*

Randles, C. A., Da Silva, A. M., Buchard, V., Colarco, P. R., Darmenov, A., Govindaraju, R., Smirnov, A., Holben, B., Ferrare, R., Hair, J., Shinozuka, Y. & Flynn, C. J. (2017), 'The MERRA-2 Aerosol Reanalysis, 1980 Onward. Part I: System Description and Data Assimilation Evaluation', *Journal of Climate* **30**(17), 6823–6850.
URL: *https://journals.ametsoc.org/doi/10.1175/JCLI-D-16-0609.1*

Rao, S., Klimont, Z., Smith, S. J., Van Dingenen, R., Dentener, F., Bouwman, L., Riahi, K., Amann, M., Bodirsky, B. L., Van Vuuren, D. P., Aleluia Reis, L., Calvin, K., Drouet, L., Fricko, O., Fujimori, S., Gernaat, D., Havlik, P., Harmsen, M., Hasegawa, T., Heyes, C., Hilaire, J., Luderer, G., Masui, T., Stehfest, E., Strefler, J., Van Der Sluis, S. & Tavoni, M. (2017), 'Future air pollution in the Shared Socio-economic Pathways', *Global Environmental Change* **42**, 346–358.
URL: *https://linkinghub.elsevier.com/retrieve/pii/S0959378016300723*

Rodgers, K. B., Lee, S.-S., Rosenbloom, N., Timmermann, A., Danabasoglu, G., Deser, C., Edwards, J., Kim, J.-E., Simpson, I. R., Stein, K., Stuecker, M. F., Yamaguchi, R., Bódai, T., Chung, E.-S., Huang, L., Kim, W. M., Lamarque, J.-F., Lombardozzi, D. L., Wieder, W. R. & Yeager, S. G. (2021), 'Ubiquity of human-induced changes in climate variability', *Earth System Dynamics* **12**(4), 1393–1411.
URL: *https://esd.copernicus.org/articles/12/1393/2021/*

Samset, B. H., Lund, M. T., Bollasina, M., Myhre, G. & Wilcox, L. (2019), 'Emerging Asian aerosol patterns', *Nature Geoscience* **12**(8), 582–584.
URL: *https://www.nature.com/articles/s41561-019-0424-5*

Samset, B. H., Sand, M., Smith, C. J., Bauer, S. E., Forster, P. M., Fuglestvedt, J. S., Osprey, S. & Schleussner, C. (2018), 'Climate Impacts From a Removal of Anthropogenic Aerosol Emissions', *Geophysical Research Letters* **45**(2), 1020–1029.
URL: *https://agupubs.onlinelibrary.wiley.com/doi/10.1002/2017GL076079*

Samset, B. H., Wilcox, L. J., Allen, R. J., Stjern, C. W., Lund, M. T., Ahmadi, S., Ekman, A., Elling, M. T., Fraser-Leach, L., Griffiths, P., Keeble, J., Koshiro, T., Kushner, P., Lewinschal, A., Makkonen, R., Merikanto, J., Nabat, P., Narazenko, L., O'Donnell, D., Oshima, N., Rumbold, S. T., Takemura, T., Tsigaridis, K. & Westervelt, D. M. (2025), 'East Asian aerosol cleanup has likely contributed to the recent acceleration in global warming', *Communications Earth & Environment* **6**(1).
URL: *https://www.nature.com/articles/s43247-025-02527-3*

Seneviratne, S. I., Zhang, X., Adnan, M., Badi, W., Dereczynski, C., Di Luca, A., Ghosh, S., Iskandar, I., Kossin, J., Lewis, S., Otto, F., Pinto, I., Satoh, M., Vicente-Serrano, S. M., Wehner, M., Zhou, B., Masson-Delmotte, V., Zhai, P., Pirani, A., Connors, S. L., Péan, C., Berger, S., Caud, N., Chen, Y., Goldfarb, L., Gomis, M. I., Huang, M., Leitzell, K., Lonnoy, E., Matthews, J. B. R., Maycock, T. K., Waterfield, T., Yelekçi, O., Yu, R. & Zhou, B. (2021), Weather and Climate Extreme Events in a Changing Climate, *in* 'Climate Change 2021: The Physical Science Basis. Contribution of Working Group I to the Sixth Assessment Report of the Intergovernmental Panel on Climate Change', Cambridge University Press, Cambridge, United Kingdom and New York, NY, USA, pp. 1513–1766.

Simpson, I. R., Rosenbloom, N., Danabasoglu, G., Deser, C., Yeager, S. G., McCluskey, C. S., Yamaguchi, R., Lamarque, J.-F., Tilmes, S., Mills, M. J. & Rodgers, K. B. (2023), 'The CESM2 Single-Forcing Large Ensemble and Comparison to CESM1: Implications for Experimental Design', *Journal of Climate* **36**(17), 5687–5711.
URL: *https://journals.ametsoc.org/view/journals/clim/36/17/JCLI-D-22-0666.1.xml*

Thompson, V., Mitchell, D., Hegerl, G. C., Collins, M., Leach, N. J. & Slingo, J. M. (2023), 'The most at-risk regions in the world for high-impact heatwaves', *Nature Communications* **14**(1), 2152.
URL: *https://www.nature.com/articles/s41467-023-37554-1*

Tobías, A., Hashizume, M., Honda, Y., Sera, F., Ng, C. F. S., Kim, Y., Roye, D., Chung, Y., Dang, T. N., Kim, H., Lee, W., Íñiguez, C., Vicedo-Cabrera, A., Abrutzky, R., Guo, Y., Tong, S., Coelho, M. D. S. Z. S., Saldiva, P. H. N., Lavigne, E., Correa, P. M., Ortega, N. V., Kan, H., Osorio, S., Kyselý, J., Urban, A., Orru, H., Indermitte, E., Jaakkola, J. J. K., Ryti, N. R. I., Pascal, M., Huber, V., Schneider, A., Katsouyanni, K., Analitis, A., Entezari, A., Mayvaneh, F., Goodman, P., Zeka, A., Michelozzi, P., de'Donato, F., Alahmad, B., Diaz, M. H., De La

Cruz Valencia, C., Overcenco, A., Houthuijs, D., Ameling, C., Rao, S., Di Ruscio, F., Carrasco, G., Seposo, X., Nunes, B., Madureira, J., Holobaca, I.-H., Scovronick, N., Acquaotta, F., Forsberg, B., Åström, C., Ragettli, M. S., Guo, Y.-L. L., Chen, B.-Y., Li, S., Colistro, V., Zanobetti, A., Schwartz, J., Dung, D. V., Armstrong, B. & Gasparrini, A. (2021), 'Geographical Variations of the Minimum Mortality Temperature at a Global Scale: A Multicountry Study', *Environmental Epidemiology* **5**(5), e169.
URL: *https://journals.lww.com/10.1097/EE9.0000000000000169*

Van Der A, R. J., Mijling, B., Ding, J., Koukouli, M. E., Liu, F., Li, Q., Mao, H. & Theys, N. (2017), 'Cleaning up the air: effectiveness of air quality policy for SO_2 and NO x emissions in China', *Atmospheric Chemistry and Physics* **17**(3), 1775–1789.
URL: *https://acp.copernicus.org/articles/17/1775/2017/*

Wang, Y., Jiang, J. H. & Su, H. (2015), 'Atmospheric responses to the redistribution of anthropogenic aerosols', *Journal of Geophysical Research: Atmospheres* **120**(18), 9625–9641.
URL: *https://agupubs.onlinelibrary.wiley.com/doi/10.1002/2015JD023665*

Wang, Z., Lin, L., Xu, Y., Che, H., Zhang, X., Zhang, H., Dong, W., Wang, C., Gui, K. & Xie, B. (2021), 'Incorrect Asian aerosols affecting the attribution and projection of regional climate change in CMIP6 models', *npj Climate and Atmospheric Science* **4**(1), 2.
URL: *https://www.nature.com/articles/s41612-020-00159-2*

Wergen, G. & Krug, J. (2010), 'Record-breaking temperatures reveal a warming climate', *EPL (Europhysics Letters)* **92**(3), 30008.
URL: *https://iopscience.iop.org/article/10.1209/0295-5075/92/30008*

Westervelt, D. M., Mascioli, N. R., Fiore, A. M., Conley, A. J., Lamarque, J.-F., Shindell, D. T., Faluvegi, G., Previdi, M., Correa, G. & Horowitz, L. W. (2020), 'Local and remote mean and extreme temperature response to regional aerosol emissions reductions', *Atmospheric Chemistry and Physics* **20**(5), 3009–3027.
URL: *https://acp.copernicus.org/articles/20/3009/2020/*

Wilcox, L. J., Allen, R. J., Samset, B. H., Bollasina, M. A., Griffiths, P. T., Keeble, J., Lund, M. T., Makkonen, R., Merikanto, J., O'Donnell, D., Paynter, D. J., Persad, G. G., Rumbold, S. T., Takemura, T., Tsigaridis, K., Undorf, S. & Westervelt, D. M. (2023), 'The Regional Aerosol Model Intercomparison Project (RAMIP)', *Geoscientific Model Development* **16**(15), 4451–4479.
URL: *https://gmd.copernicus.org/articles/16/4451/2023/*

Zheng, B., Tong, D., Li, M., Liu, F., Hong, C., Geng, G., Li, H., Li, X., Peng, L., Qi, J., Yan, L., Zhang, Y., Zhao, H., Zheng, Y., He, K. & Zhang, Q. (2018), 'Trends in China's anthropogenic emissions since 2010 as the consequence of clean air actions', *Atmospheric Chemistry and Physics* **18**(19), 14095–14111.
URL: *https://acp.copernicus.org/articles/18/14095/2018/*

Supplementary Material: Regional anthropogenic aerosol reductions amplify probability of record-breaking heat extremes

Florian Kraulich[1,*], Peter Pfleiderer[1], Sharar Ahmadi[2], Robert J. Allen[3], Pierre Nabat[4], Geeta G. Persad[5], Bjørn H. Samset[6], Laura J. Wilcox[2] and Sebastian Sippel[1]

[1]Institute for Meteorology, Leipzig University; Leipzig, Germany

[2]National Centre for Atmospheric Science, University of Reading; Reading, United Kingdom

[3]Department of Earth and Planetary Sciences, University of California Riverside; Riverside CA, USA

[4]Météo-France, CNRS, Univ. Toulouse, CNRM; Toulouse, France

[5]Department of Earth and Planetary Science, The University of Texas at Austin; Austin, USA

[6]CICERO Center for International Climate Research; Oslo, Norway

[*]Author to whom any correspondence should be addressed.

Supplementary Figures

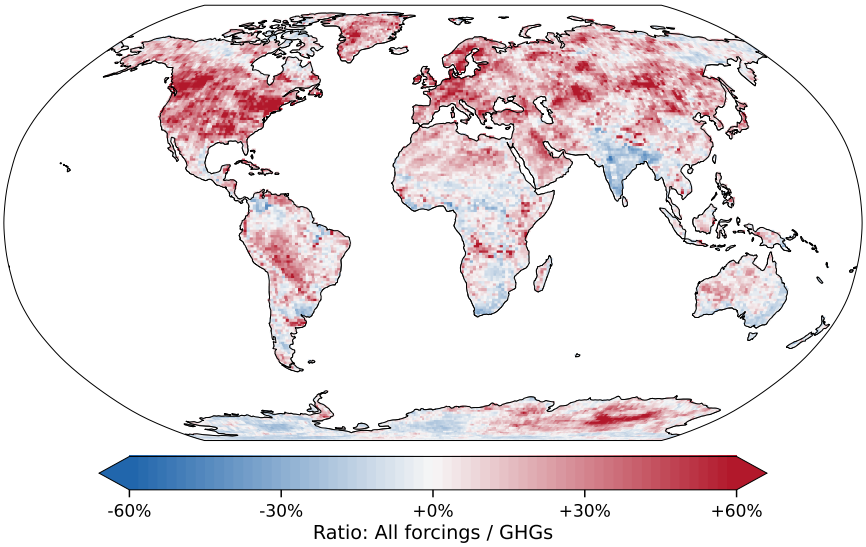

Supplementary Figure 1: Maps of ratio between 31-year smoothed empirically derived annual record-breaking probability in the CESM2 large ensemble and the GHG-only simulations from the CESM2 single-forcing large ensemble for the year 2026.

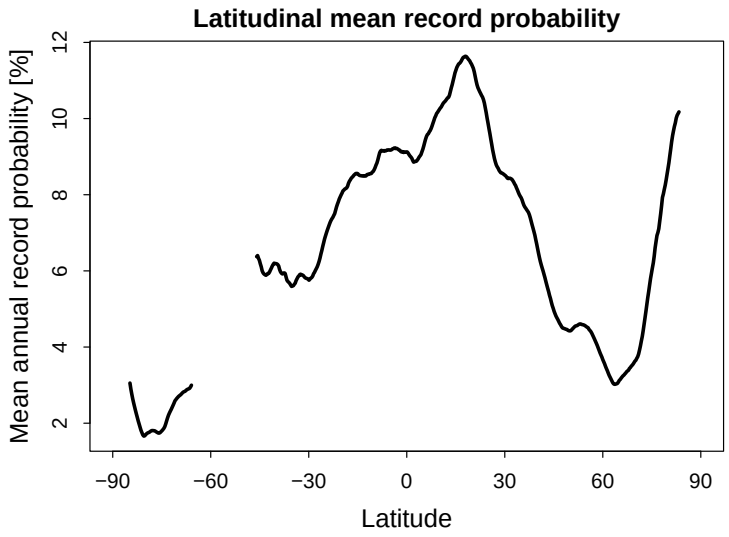

Supplementary Figure 2: Latitudinal mean annual record-breaking probability of hottest 7-day period of daily mean temperatures (TM7d) records over land in ERA5 for period from 2010 to 2025. The profile is smoothed with a 10° latitude window, and records are defined relative to the maximum in the preceding 50-year period.

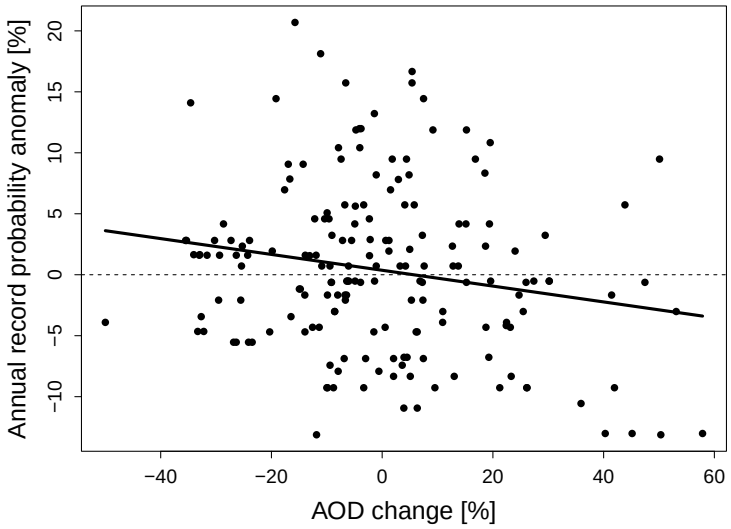

Supplementary Figure 3: Annual probability anomaly of hottest 7-day period of daily mean temperature (TM7d) records in reanalysis data with respect to the latitudinal mean annual record probability from 2010 to 2025 vs. change in total aerosol optical depth (AOD) from 1980–2009 to 2010–2025 of 5°× 5° land regions where average AOD > 0.2, resulting in 178 eligible regions. Records are defined relative to the maximum in the preceding 50-year period. The black line shows the linear regression showing a statistically significant slope of -0.6 percentage points in annual record probability anomaly per 10% change in total AOD.

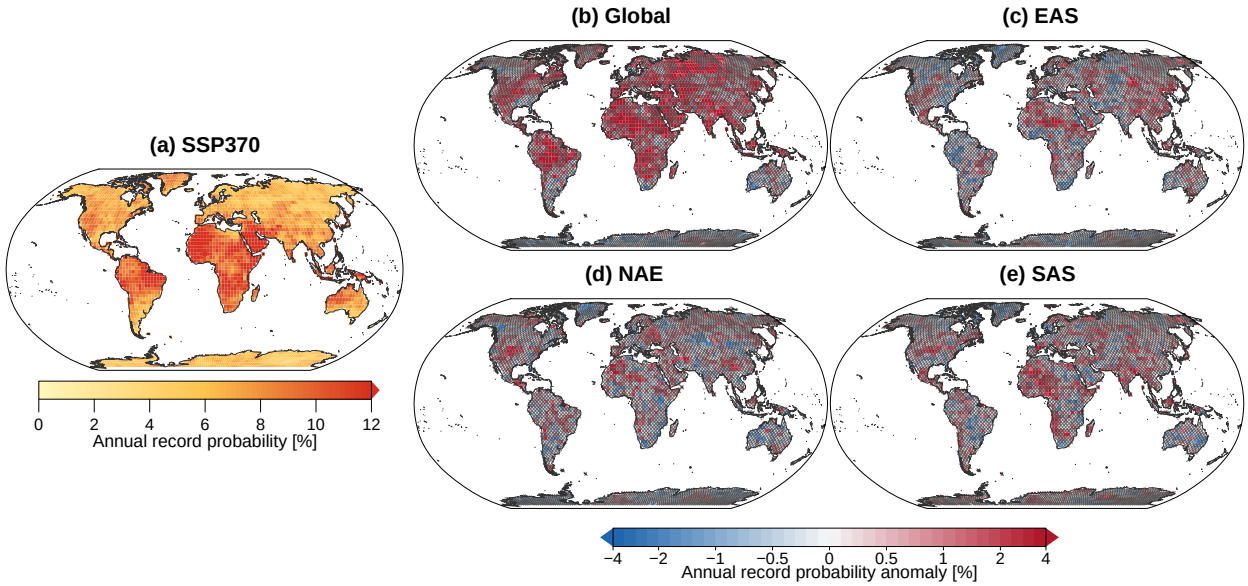

Supplementary Figure 4: Annual probability of empirically derived record-breaking heat extremes of hottest 7-day period of daily maximum temperatures (TX7d) in the Regional Aerosol Model Intercomparison Project (RAMIP) for the period 2041–2050, with records defined relative to the preceding annual maxima since 2015 within each simulation.. (a) Absolute annual record-breaking heat probability in the SSP3-7.0 reference scenario. (b)–(e) Annual record-breaking heat probability anomaly with respect to SSP3-7.0 for different RAMIP scenarios, where anthropogenic aerosols follow the SSP1-2.6 scenario either globally or only in selected regions, namely North America and Europe, East Asia, and South Asia. Hatching indicates grid cells where fewer than 8 out of the 10 models agree on the sign of change as a measure of robustness.

Supplementary Tables

Supplementary Table 1: RAMIP models and their minimum number of simulations for daily maximum temperatures, RAMIP data reference and model reference (the RAMIP models that are not yet publicly available are expected to be public before publication).

Model	Simulations	RAMIP data reference	Model reference
CanESM5-1	10	Fraser-Leach et al. (2025)	Sigmond et al. (2023)
CESM2	10	Allen (2026)	Danabasoglu et al. (2020)
CNRM-ESM2-1	3	Nabat (2026)	Séférian et al. (2019)
EC-Earth3-AerChem	10	O'Donnell et al. (2025)	Van Noije et al. (2021)
GFDL-SPEAR_LO	10	not yet publicly available	Delworth et al. (2020)
GISS-E2-1-G	10	not yet publicly available	Kelley et al. (2020)
MIROC6	10	not yet publicly available	Tatebe et al. (2019)
MRI-ESM2-0	10	Oshima and Koshiro (2025)	Yukimoto et al. (2019)
NorESM2-LM	7	Lewinschal (2025)	Seland et al. (2020)
UKESM1-0-LL	10	Rumbold et al. (2026)	Sellar et al. (2019)

Supplementary Table 2: Individual model anomalies of the Regional Aerosol Model Intercomparison Project (RAMIP) in annual probability of analytically derived record-breaking heat extremes of hottest 7-day period of daily maximum temperatures (TX7d) for selected regions, namely Central Europe (CEU), East China (EAC), and Eastern Indo-Gangetic Plain (IGP). The anomalies are calculated for the period 2041–2050, with records defined relative to the preceding annual maxima since 2015 within each simulation. Values show the mean anomaly in percentage points relative to SSP3-7.0, with 2.5–97.5% bootstrap intervals in brackets. For each selected regions, the global aerosol reduction from SSP3-7.0 to SSP1-2.6 and the respective regional aerosol reductions, specifically in North America and Europe (SSP370-NAE126aer) for CEU, in East Asia (SSP370-EAS126aer) for EAC, and South Asia (SSP370-SAS126) for IGP, are shown.

	CEU		EAC		IGP	
Model	Global	Regional	Global	Regional	Global	Regional
CanESM5-1	1.0 [−4.9, 6.9]	−4.3 [−9.4, 1.6]	−7.3 [−11.9, 0.4]	−7.1 [−12.1, −0.5]	5.5 [2.5, 9.4]	1.8 [−0.9, 4.2]
CESM2	2.2 [−2.1, 7.6]	0.9 [−2.8, 4.3]	3.4 [−2.9, 8.2]	−0.7 [−4.7, 3.7]	3.9 [−0.2, 8.1]	−1.8 [−4.0, 1.6]
CNRM-ESM2-1	−0.9 [−5.0, 1.4]	−4.7 [−6.0, 0.0]	0.1 [−1.5, 6.7]	2.4 [0.0, 9.0]	3.7 [0.0, 10.0]	1.7 [−1.9, 3.0]
EC-Earth3-AerChem	4.9 [−0.6, 5.8]	9.5 [2.5, 12.6]	3.9 [2.3, 15.2]	0.9 [−2.0, 9.6]	7.3 [−2.6, 16.2]	2.0 [−2.7, 8.2]
GFDL-SPEAR_LO	−1.9 [−5.3, 1.5]	−1.9 [−5.7, 1.4]	0.6 [−3.8, 5.3]	−2.2 [−6.5, 3.1]	4.8 [0.7, 8.7]	3.1 [0.7, 5.3]
GISS-E2-1-G	−2.3 [−4.5, 0.1]	−0.3 [−3.7, 3.1]	0.1 [−3.4, 4.2]	2.0 [−1.1, 5.8]	0.5 [−4.3, 5.6]	−1.3 [−5.0, 2.8]
MIROC6	2.8 [−1.8, 6.8]	−0.2 [−3.8, 4.1]	1.6 [−0.8, 5.2]	2.2 [−0.7, 4.9]	3.3 [0.3, 6.0]	1.7 [−1.1, 4.0]
MRI-ESM2-0	−0.4 [−3.5, 3.9]	−1.1 [−3.7, 2.2]	2.3 [−3.2, 6.6]	6.4 [1.5, 10.6]	6.2 [2.4, 10.1]	3.3 [0.8, 4.9]
NorESM2-LM	3.1 [−2.8, 9.8]	0.4 [−3.5, 2.3]	1.0 [−2.6, 8.3]	1.3 [−5.2, 6.7]	4.8 [1.3, 7.1]	1.5 [−3.2, 5.6]
UKESM1-0-LL	−0.5 [−4.0, 3.1]	−0.7 [−5.2, 4.3]	−2.2 [−6.1, 2.7]	0.8 [−5.2, 6.5]	7.2 [1.9, 14.4]	5.1 [1.4, 8.4]

References

Allen, R. (2026), 'CESM2 output prepared for the Regional Aerosol Model Intercomparison Project (RAMIP). NERC EDS Centre for Environmental Data Analysis'.
URL: *https://catalogue.ceda.ac.uk/uuid/b7c87e4dafcc486ba1eca2abac752abf/*

Danabasoglu, G., Lamarque, J., Bacmeister, J., Bailey, D. A., DuVivier, A. K., Edwards, J., Emmons, L. K., Fasullo, J., Garcia, R., Gettelman, A., Hannay, C., Holland, M. M., Large, W. G., Lauritzen, P. H., Lawrence, D. M., Lenaerts, J. T. M., Lindsay, K., Lipscomb, W. H., Mills, M. J., Neale, R., Oleson, K. W., Otto-Bliesner, B., Phillips, A. S., Sacks, W., Tilmes, S., Van Kampenhout, L., Vertenstein, M., Bertini, A., Dennis, J., Deser, C., Fischer, C., Fox-Kemper, B., Kay, J. E., Kinnison, D., Kushner, P. J., Larson, V. E., Long, M. C., Mickelson, S., Moore, J. K., Nienhouse, E., Polvani, L., Rasch, P. J. and Strand, W. G. (2020), 'The Community Earth System Model Version 2 (CESM2)', *Journal of Advances in Modeling Earth Systems* **12**(2), e2019MS001916.
URL: *https://agupubs.onlinelibrary.wiley.com/doi/10.1029/2019MS001916*

Delworth, T. L., Cooke, W. F., Adcroft, A., Bushuk, M., Chen, J., Dunne, K. A., Ginoux, P., Gudgel, R., Hallberg, R. W., Harris, L., Harrison, M. J., Johnson, N., Kapnick, S. B., Lin, S., Lu, F., Malyshev, S., Milly, P. C., Murakami, H., Naik, V., Pascale, S., Paynter, D., Rosati, A., Schwarzkopf, M., Shevliakova, E., Underwood, S., Wittenberg, A. T., Xiang, B., Yang, X., Zeng, F., Zhang, H., Zhang, L. and Zhao, M. (2020), 'SPEAR: The Next Generation GFDL Modeling System for Seasonal to Multidecadal Prediction and Projection', *Journal of Advances in Modeling Earth Systems* **12**(3), e2019MS001895.
URL: *https://agupubs.onlinelibrary.wiley.com/doi/10.1029/2019MS001895*

Fraser-Leach, L., Kushner, P., von Salzen, K. and Swart, N. (2025), 'CanESM5-1 output prepared for the Regional Aerosol Model Intercomparison Project (RAMIP). NERC EDS Centre for Environmental Data Analysis'.
URL: *https://catalogue.ceda.ac.uk/uuid/a33a7cc2d0a84e27a78b24d70fe257e4/*

Kelley, M., Schmidt, G. A., Nazarenko, L. S., Bauer, S. E., Ruedy, R., Russell, G. L., Ackerman, A. S., Aleinov, I., Bauer, M., Bleck, R., Canuto, V., Cesana, G., Cheng, Y., Clune, T. L., Cook, B. I., Cruz, C. A., Del Genio, A. D., Elsaesser, G. S., Faluvegi, G., Kiang, N. Y., Kim, D., Lacis, A. A., Leboissetier, A., LeGrande, A. N., Lo, K. K., Marshall, J., Matthews, E. E., McDermid, S., Mezuman, K., Miller, R. L., Murray, L. T., Oinas, V., Orbe, C., García-Pando, C. P., Perlwitz, J. P., Puma, M. J., Rind, D., Romanou, A., Shindell, D. T., Sun, S., Tausnev, N., Tsigaridis, K., Tselioudis, G., Weng, E., Wu, J. and Yao, M. (2020), 'GISS-E2.1: Configurations and Climatology', *Journal of Advances in Modeling Earth Systems* **12**(8), e2019MS002025.
URL: *https://agupubs.onlinelibrary.wiley.com/doi/10.1029/2019MS002025*

Lewinschal, A. (2025), 'NorESM2-LM output prepared for the Regional Aerosol Model Intercomparison Project (RAMIP). NERC EDS Centre for Environmental Data Analysis'.
URL: *https://catalogue.ceda.ac.uk/uuid/44100d99d120487284d7b778dbc76bdf/*

Nabat, P. (2026), 'CNRM-ESM2-1 output prepared for the Regional Aerosol Model Intercomparison Project (RAMIP). NERC EDS Centre for Environmental Data Analysis'.
URL: *https://catalogue.ceda.ac.uk/uuid/5477e60b209a4e169ca60d7f01a017eb/*

O'Donnell, D., Makkonen, R. and Merikanto, J. (2025), 'EC-Earth3-AerChem output prepared for the Regional Aerosol Model Intercomparison Project (RAMIP). NERC EDS Centre for Environmental Data Analysis'.
URL: *https://catalogue.ceda.ac.uk/uuid/d581329422fb455ab9af0ea96c04d266/*

Oshima, N. and Koshiro, T. (2025), 'MRI-ESM2-0 output prepared for the Regional Aerosol Model Intercomparison Project (RAMIP). NERC EDS Centre for Environmental Data Analysis'.
URL: *https://catalogue.ceda.ac.uk/uuid/e8678aaf39144d8cb10cd02e8a562101/*

Rumbold, S., Keeble, J., Wilcox, L., Ahmadi, S., Griffiths, P., Lister, G. and Predoi, V. (2026), 'UKESM1-0-LL output prepared for the Regional Aerosol Model Intercomparison Project (RAMIP). NERC EDS Centre for Environmental Data Analysis'.
URL: *https://catalogue.ceda.ac.uk/uuid/63233813672245a2ba3c6de90c4cfaee/*

Seland, O., Bentsen, M., Olivié, D., Toniazzo, T., Gjermundsen, A., Graff, L. S., Debernard, J. B., Gupta, A. K., He, Y.-C., Kirkevåg, A., Schwinger, J., Tjiputra, J., Aas, K. S., Bethke, I., Fan, Y., Griesfeller, J., Grini, A., Guo, C., Ilicak, M., Karset, I. H. H., Landgren, O., Liakka, J., Moseid, K. O., Nummelin, A., Spensberger, C., Tang, H., Zhang, Z., Heinze, C., Iversen, T. and Schulz, M. (2020), 'Overview of the Norwegian Earth System Model (NorESM2) and key climate response of CMIP6 DECK, historical, and scenario simulations', *Geoscientific Model Development* **13**(12), 6165–6200.
URL: *https://gmd.copernicus.org/articles/13/6165/2020/*

Sellar, A. A., Jones, C. G., Mulcahy, J. P., Tang, Y., Yool, A., Wiltshire, A., O'Connor, F. M., Stringer, M., Hill, R., Palmieri, J., Woodward, S., de Mora, L., Kuhlbrodt, T., Rumbold, S. T., Kelley, D. I., Ellis, R., Johnson, C. E., Walton, J., Abraham, N. L., Andrews, M. B., Andrews, T., Archibald, A. T., Berthou, S., Burke, E., Blockley, E., Carslaw, K., Dalvi, M., Edwards, J., Folberth, G. A., Gedney, N., Griffiths, P. T., Harper, A. B., Hendry, M. A., Hewitt, A. J., Johnson, B., Jones, A., Jones, C. D., Keeble, J., Liddicoat, S., Morgenstern, O., Parker, R. J., Predoi, V., Robertson, E., Siahaan, A., Smith, R. S., Swaminathan, R., Woodhouse, M. T., Zeng, G. and Zerroukat, M. (2019), 'UKESM1: Description and Evaluation of the U.K. Earth System Model', *Journal of Advances in Modeling Earth Systems* **11**(12), 4513–4558. _eprint: https://agupubs.onlinelibrary.wiley.com/doi/pdf/10.1029/2019MS001739.
URL: *https://agupubs.onlinelibrary.wiley.com/doi/abs/10.1029/2019MS001739*

Sigmond, M., Anstey, J., Arora, V., Digby, R., Gillett, N., Kharin, V., Merryfield, W., Reader, C., Scinocca, J., Swart, N., Virgin, J., Abraham, C., Cole, J., Lambert, N., Lee, W.-S., Liang, Y., Malinina, E., Rieger, L., Von Salzen, K., Seiler, C., Seinen, C., Shao, A., Sospedra-Alfonso, R., Wang, L. and Yang, D. (2023), 'Improvements in the Canadian Earth System Model (CanESM) through systematic model analysis: CanESM5.0 and

CanESM5.1', *Geoscientific Model Development* **16**(22), 6553–6591.
URL: *https://gmd.copernicus.org/articles/16/6553/2023/*

Séférian, R., Nabat, P., Michou, M., Saint-Martin, D., Voldoire, A., Colin, J., Decharme, B., Delire, C., Berthet, S., Chevallier, M., Sénési, S., Franchisteguy, L., Vial, J., Mallet, M., Joetzjer, E., Geoffroy, O., Guérémy, J., Moine, M., Msadek, R., Ribes, A., Rocher, M., Roehrig, R., Salas-y-Mélia, D., Sanchez, E., Terray, L., Valcke, S., Waldman, R., Aumont, O., Bopp, L., Deshayes, J., Éthé, C. and Madec, G. (2019), 'Evaluation of CNRM Earth System Model, CNRM-ESM2-1: Role of Earth System Processes in Present-Day and Future Climate', *Journal of Advances in Modeling Earth Systems* **11**(12), 4182–4227.
URL: *https://agupubs.onlinelibrary.wiley.com/doi/10.1029/2019MS001791*

Tatebe, H., Ogura, T., Nitta, T., Komuro, Y., Ogochi, K., Takemura, T., Sudo, K., Sekiguchi, M., Abe, M., Saito, F., Chikira, M., Watanabe, S., Mori, M., Hirota, N., Kawatani, Y., Mochizuki, T., Yoshimura, K., Takata, K., O'ishi, R., Yamazaki, D., Suzuki, T., Kurogi, M., Kataoka, T., Watanabe, M. and Kimoto, M. (2019), 'Description and basic evaluation of simulated mean state, internal variability, and climate sensitivity in MIROC6', *Geoscientific Model Development* **12**(7), 2727–2765.
URL: *https://gmd.copernicus.org/articles/12/2727/2019/*

Van Noije, T., Bergman, T., Le Sager, P., O'Donnell, D., Makkonen, R., Gonçalves-Ageitos, M., Döscher, R., Fladrich, U., Von Hardenberg, J., Keskinen, J.-P., Korhonen, H., Laakso, A., Myriokefalitakis, S., Ollinaho, P., Pérez García-Pando, C., Reerink, T., Schrödner, R., Wyser, K. and Yang, S. (2021), 'EC-Earth3-AerChem: a global climate model with interactive aerosols and atmospheric chemistry participating in CMIP6', *Geoscientific Model Development* **14**(9), 5637–5668.
URL: *https://gmd.copernicus.org/articles/14/5637/2021/*

Yukimoto, S., Kawai, H., Koshiro, T., Oshima, N., Yoshida, K., Urakawa, S., Tsujino, H., Deushi, M., Tanaka, T., Hosaka, M., Yabu, S., Yoshimura, H., Shindo, E., Mizuta, R., Obata, A., Adachi, Y. and Ishii, M. (2019), 'The Meteorological Research Institute Earth System Model Version 2.0, MRI-ESM2.0: Description and Basic Evaluation of the Physical Component', *Journal of the Meteorological Society of Japan. Ser. II* **97**(5), 931–965.
URL: *https://www.jstage.jst.go.jp/article/jmsj/97/5/97_2019-051/_article*